Research Article

Nano Research
2023, 16(7): 10522–10529

ISSN 1998-0124 CN 11-5974/O4
https://doi.org/10.1007/s12274-023-5529-x

Breaking the symmetry of colloidal 2D nanoplatelets: Twist induced quantum coupling

Zahid Nazir[1], Yingzhuo Lun[3], Jialu Li[4], Gaoling Yang[2] (✉), Mingrui Liu[1], Shuqi Li[3], Gang Tang[5], Guofeng Zhang[4] (✉), Jiawang Hong[3] (✉), Liantuan Xiao[4], and Haizheng Zhong[1]

[1] *MIIT Key Laboratory for Low-dimensional Quantum Structure and Devices, School of Materials Science & Engineering, Beijing Institute of Technology, Beijing 100081, China*
[2] *MIIT Key Laboratory for Low-dimensional Quantum Structure and Devices, School of Optics and Photonics, Beijing Institute of Technology, Beijing 100081, China*
[3] *School of Aerospace Engineering, Beijing Institute of Technology, Beijing 100081, China*
[4] *State Key Laboratory of Quantum Optics and Quantum Optics Devices, Institute of Laser Spectroscopy, Collaborative Innovation Center of Extreme Optics, Shanxi University, Taiyuan 030006, China*
[5] *Advanced Research Institute of Multidisciplinary Science, Beijing Institute of Technology, Beijing 100081, China*

Received: 19 November 2022 / **Revised:** 10 January 2023 / **Accepted:** 25 January 2023

ABSTRACT

Twist provides a new degree of freedom for nanomaterial modifications, which can provide novel physical properties. Here, colloidal two-dimensional (2D) twisted CdSe nanoplatelets (NPLs) are successfully fabricated and their morphology can change from totally flat to edge-twisted, and then to middle-twisted with prolonged reaction time. By combining experiments and corresponding theoretical analyses, we have established the length-dependent relationships between the surface energy and twist, with a critical lateral dimension of 30 nm. We found that the defects formed during the synthesis process play a vital role in generating intense stress that develops a strong torsion tensor around the edges, resulting in edge-twisted and final middle-twisted NPLs. Furthermore, due to the geometric asymmetry of twisted NPLs, the dissymmetry factor of single particle NPLs can reach up to 0.334. Specifically, quantum coupling occurs in middle-twisted NPLs by twisting one parent NPL into two daughter NPLs, which are structurally and electronically coupled. This work not only further deepens our understanding of the twist mechanism of 2D NPLs during colloidal synthesis, but also opens a pathway for applications using twistronics and quantum technology.

KEYWORDS

nanoplatelets, CdSe, twist, circular dichroism, quantum coupling

1 Introduction

Twist, one of the most fascinating geometries in the natural world, has been observed for a number of synthetic materials, playing a peculiar role in the fundamental fields of physics, chemistry, biology, and materials science [1–5]. In particular, twist has recently emerged as a promising new degree of freedom for one-dimensional (1D) and two-dimensional (2D) nanomaterial modifications, introducing novel physical properties, such as Hofstadter's spectra [6, 7], unconventional superconductivity [8], moiré excitons [9], tunneling conductance [10], and nonlinear optics [11], etc. Precisely controlling the twist angle of 2D materials can effectively change the crystal symmetry and tailor the interlayer coupling strength of twisted multilayers. To achieve a twist in nanomaterials, internal or external driving forces are mandatory, where transfer methods [8, 10], atomic force microscope tip manipulation techniques [12], or micromechanically stacking in desired relative orientations were used [13]. However, the majority of these methods borrow external forces, and the twist that arises naturally during synthesis is still limited by poor control of internal forces. Furthermore, these systems suffer from the lack of understanding of the origin of the governing factors behind the twist, and as a result, the controls are imprecise.

Colloidal 2D semiconductor quantum wells, also known as nanoplatelets (NPLs), have recently emerged as a favorable and novel platform for optoelectronic applications, including light-emitting diodes and lasing [14–22]. Compared to other thin nanomaterials that can twist under stresses, such as graphene or transition metal dichalcogenides, colloidal NPLs are more versatile, and their thickness, composition, and lateral dimensions can be varied to tune their optoelectronic properties [23]. Recently, increasing evidence suggests that NPLs may curl into scrolls, helices, and twists, which are predicted to favor peculiar optical properties, such as circularly polarized light [24–30]. Despite the progress made, the in-depth understanding or physical explanation of such structural curvature is still lacking [31]. This is partly since almost all past reports have focused on the influence of the surface stress induced by the surface ligands [32], which are absorbed onto the crystalline surface and deform the inorganic core, whereas only a few recent reports have studied the surface

Address correspondence to Gaoling Yang, glyang@bit.edu.cn; Guofeng Zhang, guofeng.zhang@sxu.edu.cn; Jiawang Hong, hongjw@bit.edu.cn

defects-induced stress variation and its effect on the shape and optical properties of NPLs [14]. Especially in the case of 2D NPLs with high fractions of surface atoms that are synthesized by colloidal method, surface defects play a major and non-ignorable inducement for the twist, providing an attractive alternative platform for further promoting the understanding of the fundamental mechanism underlying internal stress-induced twists in colloidal NPLs.

Here, we introduce breaking the symmetry of 2D CdSe NPLs by twist, which evolves naturally during the colloidal synthesis process in the solution phase. With the growth of NPLs, the morphology of NPLs changes from totally flat to edge-twisted, and then to middle-twisted. Both experimental observations and associated theoretical analysis indicate that the twist is length-dependent, where the critical length for twist is calculated to be 30 nm. We further explore the vital role of surface defects in twist formation. Moreover, circularly polarized excitation studies were performed on the middle-twisted NPLs using single-particle spectroscopy, and the dissymmetry factor can reach up to 0.334, which is much larger than that of chiral NPLs produced by the ligand exchange method. Impressively, the quantum coupling is discerned in the middle twisted NPLs by the redshift of the band gap transitions as well as single-particle spectroscopy studies. Considering the variety of novel and fantastic physical properties of twisted NPLs, such as chirality and quantum coupling, our work creates a framework for the further development of twistronics, quantum technologies, and optoelectronic applications.

2 Experimental

2.1 Synthesis of cadmium myristate

Cadmium myristate ($Cd(Myr)_2$) was prepared as reported elsewhere. Typically, 1.54 g (5 mmol) of cadmium nitrate tetrahydrate ($Cd(NO_3)_2{\cdot}4H_2O$) was dissolved in 40 mL methanol by stirring. In a separate beaker, 3.13 g (12.5 mmol) of sodium myristate was dissolved in 250 mL of methanol by stirring for 1 h. After complete dissolution, $Cd(NO_3)_2$ solution was slowly added to the sodium myristate solution and kept for 1 h under stirring. The white precipitates of $Cd(Myr)_2$ were rinsed and washed with methanol for several times and dried under vacuum for overnight.

2.2 Synthesis of three monolayers CdSe NPLs

Three monolayers (3 ML) CdSe NPLs were synthesized as reported with few modifications [33]. In a typical 3 ML CdSe NPLs synthesis, 170 mg (0.3 mmol) of $Cd(Myr)_2$, 20.5 mg (0.26 mmol) selenium powder, 15 mL octadecene (ODE) were loaded in a 3-necked round bottom flask and subjected to vacuum at 100 °C for 1 h. The reaction was then connected to nitrogen flux and heated to 160 °C for 10 min. The color of the solution gradually turned from dark black to pale, and the temperature was raised at 10 °C/min. When the temperature approached 200 °C, 100 μL propionic acid dispersed in 1 mL ODE was swiftly injected into the solution for the nucleation of CdSe nanocrystals, as the temperature continuously kept increasing to 220 °C. The reaction was kept at 220 °C for 20 min for the growth of NPLs. After 20 min, 2 mL cadmium oleate (0.5 M) was injected into the solution, the heating mantle was removed, and the solution was cooled under air. Around 60 °C, the CdSe NPLs solution was mixed with 10 mL n-hexane and purified from unreacted precursors, and the nanoparticles were re-dispersed in hexane for analyses.

2.3 Characterization methods

The transmission electron microscopy (TEM) images were taken on a JEOL 2100 TEM equipped with an LaB_6 filament at an acceleration voltage of 200 kV. High-resolution TEM (HRTEM) and scanning transmission electron microscopy (STEM) imaging were taken on a Tecnai F20 G2 microscope (Thermo Fisher Scientific) with an accelerating voltage of 200 kV. The ultraviolet–visible (UV–Vis) absorption spectra of the samples were recorded using UV–Vis/NIR spectrophotometer (V-670, JASCO). The photoluminescence (PL) spectra were measured with a fluorescence spectrophotometer (SpectraScan, PR-655) with an excitation wavelength of 365 nm.

2.4 Single particle optical measurements

Single particle measurements were performed by a homemade confocal fluorescence imaging microscope. A supercontinuum laser (EXW-12, NKT, 50–100 ps, 5 MHz repetition rate) with an acousto-optic tunable filter (SuperK VARIA) was used as the excitation light source to generate a laser with a wavelength of 405 ± 5 nm. An oil immersion objective lens (Olympus, 100x, 1.3NA) was used to excite the single NPLs sample and collect the PL photons. The PL photons passing through a dichroic mirror (Semrock) and a high-pass filter (Semrock), were focused on a 50 μm pinhole to exclude out-of-focus photons. Then, the PL photons were divided into two beams by a 50/50 beam splitter cube and finally collected by a pair of single-photon avalanche diode detectors (SPCM-AQR-15, PerkinElmer). The synchronization signal of the picosecond-pulsed laser and the arrival time of each photon was recorded by a time-tagged, time-resolved, and time-correlation single photon counting (TTTR-TCSPC) data acquisition card (HydraHarp 400, PicoQuant). With a routine written in MATLAB, we could obtain the PL intensity trajectories, decay curves, second-order correlation function curves, and fluorescence lifetime intensity distribution of single NPLs. The PL spectra of single NPLs were recorded by a spectrograph (Andor, Shamrock 500i).

2.5 Single particle circular polarization measurements

The output of the supercontinuum laser with 405 nm was filtered by a Glan-Taylor polarizer (GT10, extinction ratio > 100,000:1) and a broadband polarizing beamsplitter (PBS121, extinction ratio > 1000:1) was used to generate a linearly polarized light. A quarter waveplate (AQWP10M-580) converts the linearly polarized light to circularly polarized light. The right and left-handed circular polarizations were alternated by turning the fast axis of the quarter waveplate. The excitation beam was then focused on the sample using an oil immersion objective lens (Olympus, 100x, 1.3NA) to excite the single NPLs and collect the PL photons. In the transmitted light path, a long-pass emission filter was used to block the excitation beam and allowed the measurement of the luminescence of NPLs. Then, the epi-detected signal was filtered, using a dichroic mirror and a long-pass filter, and coupled into a pair of single-photon avalanche diode detectors (SPCM-AQR-15, PerkinElmer) that were connected to a time-correlated single photon counting (TCSPC) system (PicoQuant, HydraHarp 400).

3 Results and discussion

3 ML CdSe NPLs were synthesized according to a modification of previously reported procedures developed for colloidal 2D semiconductor NPLs [33], as described in detail in the Experimental section. Briefly, it involves a solution-based reaction by heating Cd carboxylate and elemental Se in ODE typically to 220 °C with the addition of a short-chain ligand at a specific nucleation temperature. It is possible to tune the width and aspect ratio of NPLs by varying the chain lengths of Cd carboxylate precursors and growth conditions. The TEM image in Fig. 1(d) indicates that uniform flat NPLs with a width of 6 nm and a

length of 28 nm were formed at a growth time of 3 min, which is also clearly observed by the high-angle annular dark-field scanning TEM (HAADF-STEM) characterization. At 5 min, the length of the obtained NPLs increased to 40 nm, while most of them exhibited twist at the edge of the NPL (Fig. 1(e)), which could be more clearly observed by high-resolution STEM (Fig. 1(h)). This edge-twist effect also explains the apparent width variations observed along the NPLs. The width of the NPLs reduced three times from 6 to approximately 2 nm, as can be seen from the width and length statistics in Fig. 1(k). After 10 min of reaction, no remarkable changes in the length of the NPLs have been observed, and almost all the NPLs underwent twist, and majority of which were located in the middle (Figs. 1(f) and 1(i)). From the size statistics shown in Fig. 1(l), the width of the NPLs shortens from 6 to 2 nm near the middle, and then bounces back to 6 nm upon reaching the opposite end, coinciding with the middle-twist effect. Their corresponding histograms of the twist probability of NPLs are reflected in Figs. 1(m)–1(o), from which we can clearly see that with extending the growth time, the NPLs change from flat to edge-twist, then to middle-twist. It is noted that the size distribution analysis was based on the observations of 200 NPLs for each sample, and thus TEM images obtained in a larger scale containing more NPLs are shown in Fig. S1 in the Electronic Supplementary Material (ESM). These twisted NPLs are stable, and they will not turn back to untwisted ones after being fabricated, as the twist is due to the lattice and morphology variation, and twist induced the helical atomic arrangement along the crystallographic directions, which leads to the crystallographic change in a periodic lattice. These results present a structural evolution of the isolated 3 ML CdSe NPLs from totally flat to edge-twist and then to middle-twist during their growth in colloidal solution.

Now the question arises why these NPLs are prone to twist the structures into a distorted model rather than keeping their completely planar geometry. We have established a theoretical model to investigate the twist of NPLs (details of the model can be found in the ESM). The model demonstrates that the spontaneous twist in NPLs is predominantly driven by the compressive edge stress. As shown in Fig. 2(a), the twist angle θ-dependent total energy curve is calculated for the NPLs with a short length of 28 nm (growth time of 3 min), and the minimum energy at zero twist angle indicates that the planar geometry without twist is the most stable state for short NPLs. However, with the increase of the NPLs length (40 nm), the total energy curve transforms into a double-well potential with two symmetric minima away from θ = 0, driven by the compressive edge stress. Thus, the twist becomes the most energetically favorable state. Therefore, both internal and external forces which we will discuss later would result in a non-zero critical strain, below which the NPLs twist. While this effect is prominent in longer-length NPLs, it arguably diminishes in the case of relatively short NPLs. The dependence of twist angle on the length originates from the competition between bulk and edge energies. We further calculated the critical length for twisted NPLs as 30 nm, as shown in Fig. 2(b), which is also within minutes of the initial rapid growth of the NPLs. When the length of the NPLs gradually elongates and exceeds the critical length, the imbalance of compressive stress along the lateral length leads to instability, where the NPLs need to lower their energy and give rise to the torque for twist on the edge. In order to fully release the superfluous surface energy, the NPLs tend to twist into helical structures along the length direction, forming a new low-energy equilibrium state.

Since the twist is created during the synthesis process, surface strain may be caused by both the surface-absorbed ligands and defects formed during the growth process. On one hand, the self-assembly absorbed ligands on the surface can induce surface stress on the crystalline surface due to the asymmetrical organometallic bonds, which will distort the surface crystallinity [24, 32]. On the other hand, the stresses can also come from any kind of defects formed during the growth process that cause the internal trapped stresses [2], which tend to be released at elevated temperatures and usually result in twisting or rolling on their way out. Since the ligand-induced variation of surface stress and their effect on the twist or rolling of NPLs have been discussed in some studies over the past few years [24, 32], we here focus more on the effect of defects. Once the growth of an individual NPL is complete, both ends of CdSe NPL lack ligands and are exposed. These uncovered facets contain defects that are more concentrated along the edges of the NPLs having (110) facet exposed, which turn out to be the most favorable slip plane for cubic structures and further develop a strong torsion tensor around the edges, resulting in rotation and final twist of NPLs.

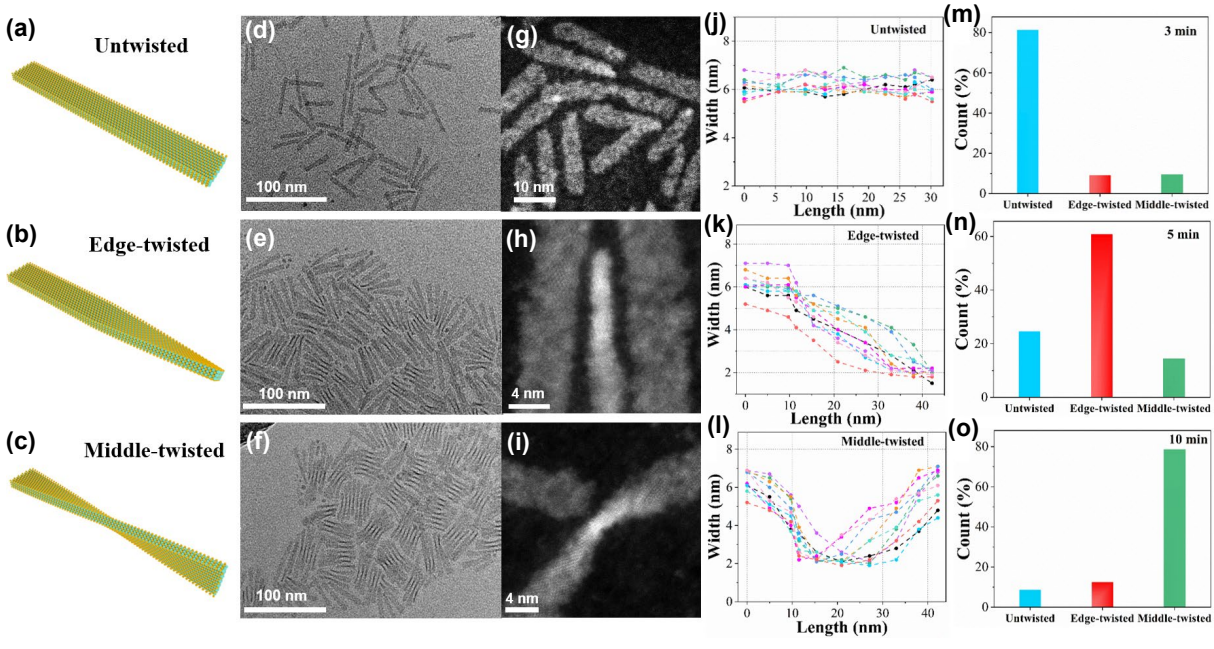

Figure 1 Twist in colloidal 2D CdSe NPLs. (a)–(c) Schematic, (d)–(f) TEM, (g)–(i) HAADF-TEM, (j)–(l) the width statistics of ten separate NPLs at different length nodes, and (m)–(o) probability distribution for untwisted, edge-twisted, and middle-twisted NPLs.

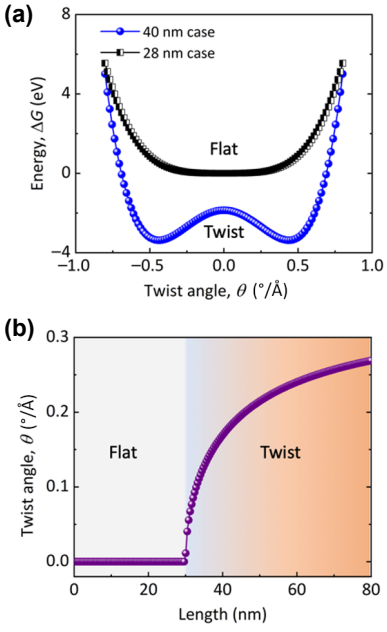

Figure 2 (a) The total energy of NPLs with different length as a function of twist angle θ. (b) The dependence of spontaneous twist angle θ on the length of NPLs. The critical length of the twist NPL is 30 nm.

The defects formed during the synthesis process play a critical role in such structure distortion, which generates strong compressive stress resulting in the twist. The thickness of 3ML CdSe NPLs is merely one nanometer [16], so the presence of vacancies or defects enables distortion in the coordination number of the unit cell and gives rise to internal stress. In addition, the missing atoms during the synthesis process may break the original charge balance of the bulk atoms, and the imbalanced charges responding to the missing atoms will rearrange themselves and tend to settle within the space between the surface atoms, giving rise to a net force mainly to the surface atoms. These forces are high enough, depending upon the concentration of vacancies, to cause the contraction of the surface, which is higher for open surfaces. We performed the first-principles calculation of finite NPLs with the absence of surface atoms and it shows the missing atoms on the surface (vacancies) cause the compressive edge stress of 0.051 eV/Å^2. Such large compressive edge stress is sufficient to drive the twist of NPLs, as demonstrated in the theoretical model in Fig. 2(a).

We have also investigated the effect of the lateral aspect ratios of NPLs on the twist of NPLs, and Fig. 3 shows the twisted structures of colloidal CdSe NPLs with larger lateral aspect ratios. NPLs with different aspect ratios were synthesized following the same procedures, which can be achieved by controlling the concentration of ligands. The TEM image in Fig. 3(a) shows the twisted NPLs with a width of 7 nm and a length of 60 nm (Fig. 3(c)), and the twisted probability reaches up to 93% (Fig. 3(e)), suggesting that nearly all the NPLs are twisted at high aspect ratios. The TEM image in Fig. 3(b) shows the twisted NPLs with a larger aspect ratio of 10 when the width was 9 nm and the length reached up to 90 nm (Fig. 3(d)), and almost all the NPLs were middle-twisted (Fig. 3(f)). This also can be proved by our theoretical model in Fig. 2(b), where the angle of twist increases with length, that is, twist is more likely to occur. Such a high twist probability further demonstrates that twist is a more stable state when NPLs exist in a larger aspect ratio. For lower aspect ratios, when the length of NPLs reaches up to a critical dimension to

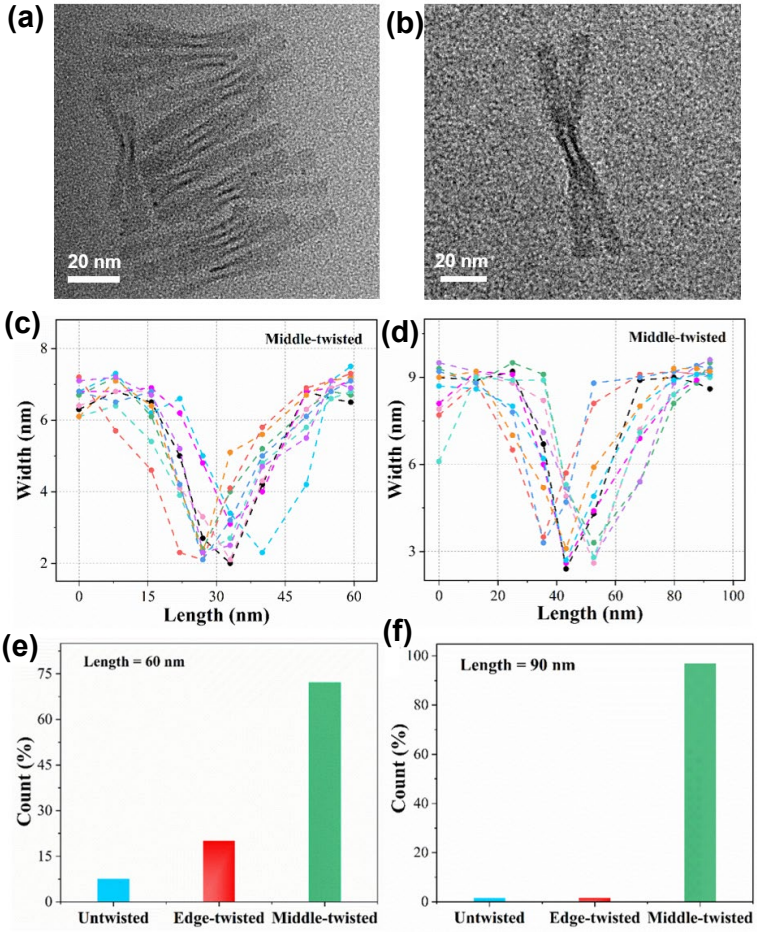

Figure 3 Twist in colloidal 2D NPLs with larger lateral aspect ratios. ((a) and (b)) TEM, ((c) and (d)) the width statistics of ten separate NPLs at different length nodes, and ((e) and (f)) twist distribution of colloidal CdSe NPLs with aspect ratios of 8.5 and 10, respectively.

release the surface energy, the NPLs tend to roll into tubes or bend into helical structures along the width or length direction, which have been reported in some literatures [24, 27]. For higher aspect ratios, since the NPLs are more flexible and mechanically unstable, and the fact that the ligand distributions on the surface are much more asymmetric, and the defects are more concentrated in the sharp edges and corners [34], which are activated at higher temperatures and prone to twist.

As these twisted CdSe NPLs possess helical atomic arrangements along the crystallographic directions, there is the possibility to trigger crystallographic or geometric chirality in periodic lattices [35, 36]. Single-particle spectroscopy based on circularly polarized excitation is a standard optical technique for studying the chirality of chiral objects [37], which measures the amount of differential absorption cross-section of chiral objects under left-handed circularly polarized light (LCP) and right-handed circularly polarized light (RCP). To explore the circularly polarized characteristics of the middle-twisted 3 ML CdSe NPLs, the single-particle circularly polarized excitation studies have been carried out at room temperature using a home-built confocal fluorescence imaging microscope. Here, we present our experimental results to probe circular dichroism of a single NPL, based on the different amounts of absorbed energy for LCP and RCP light, thus obtaining a single-particle circular dichroism PL intensity trajectories (Fig. 4), as the chiral object presents different absorption cross-sections for each handedness. For a single NPL, the only difference upon modulation is the circular polarization state, the PL intensity signal should be proportional to its difference between LCP and RCP absorption, which is exactly the circular dichroism signal we seek. Comparing the LCP PL intensity (Fig. 4(a)) with the RCP PL intensity (Fig. 4(b)), the emission maintains almost the same tracing, and a considerable intensity difference is present. Here, we use the dissymmetry factor, g, defined as $g = 2(\sigma_L - \sigma_R)/(\sigma_L + \sigma_R)$ [38], which gives a measure of the differential circular absorption cross-section normalized by the average cross-section to quantitatively characterize the degree of the circular polarization property. The average g for these single NPLs is estimated to be 0.255, which is comparable or even larger than chiral plasmonic gold nanoparticles, and much larger than chiral NPLs produced by the ligand exchange method [39, 40]. The large g factor is due to both lattice and morphology chirality, and twist induced the helical atomic arrangement along the crystallographic directions, which leads to crystallographic chirality in a periodic lattice. Moreover, as the NPLs randomly initiate twist with one-handedness in colloidal solution, nearly equal amounts of these two enantiomers make the circular dichroism spectra of NPLs solution featureless.

Twist of NPLs may give rise to new and interesting phenomena in such distinctive nanostructures, and we then consider the effect of twist on the optical properties in these NPLs. Absorption spectra of the untwisted, edge-twisted, and middle-twisted NPLs are shown in Fig. 5(a). Compared to the untwisted NPLs, the middle-twisted NPLs exhibit a considerable red-shifted absorption peak for the heavy-hole excitons, while light-hole excitons show no redshift. We attribute this red-shift to the presence of quantum coupling that hybridized the band-edge orbitals of the "two daughter NPLs" caused by twist in the middle of single NPLs and thus reduced the quantum confinement energy [41]. The magnitudes of the redshift shown in the middle-twisted NPLs is ~ 3.6 meV for the heavy-hole excitons, which is slightly lower than the 14 meV of the recently reported coupled colloidal CdSe/CdS quantum dot molecules [41], and can be attributed to the unique 1D confinement exciton in quantum wells. In addition, we observed coupling between the excited states of heavy-hole but not for the ground state of the light-hole excitons in middle-twisted quantum wells, and we believe that is because the heavy-hole excitons are predicted to show a stronger Stark shift than the light-hole excitons due to the larger effective mass of heavy-hole, which has been confirmed experimentally [42]. PL measurements can provide basic insights into the relaxation of photogenerated excitons (Fig. 5(b)). The middle-twisted NPLs show a redshift of 5.8 meV in the PL compared to the untwisted NPLs, further confirming the significant quantum coupling for the electron wave functions of two daughter NPLs in one parent NPL separated by the twist. No significant changes in the absorption and PL spectra of edge-twisted NPLs were observed, which indicate that edge twist did not change the photophysical characteristics of NPLs as no coupled NPLs were formed. Therefore, we conclude that quantum coupling occurs only in middle-twisted NPLs by twist one parent NPL into two daughter NPLs, which are structurally and electronically coupled.

To further demonstrate the quantum coupling of NPLs, the PL intensity trajectories of single untwisted, edge-twisted, and middle-twisted NPLs have been recorded at room temperature. The PL intensity trajectories of single untwisted NPLs exhibit very strong blinking, and a typical example is shown in Fig. 5(d), indicating that the single untwisted NPLs do not have a continuous on-state intensity distribution, and spend most of their time close to the dark state. Such blinking trajectory is very typical for single NPLs and has been explored in a wide range of literatures [43–45]. The PL trajectory of single edge-twisted NPLs shares nearly a similar blinking behavior and spends most of its time in the off state (Fig. 5(e)). In comparison, individual middle-twisted NPLs under similar excitation conditions present a continuous on-state distribution, as illustrated in Fig. 5(f). A similar change in the emission intermittency for coupled nanoparticles has been observed in CdSe/CdS quantum dots [41], as well as associated

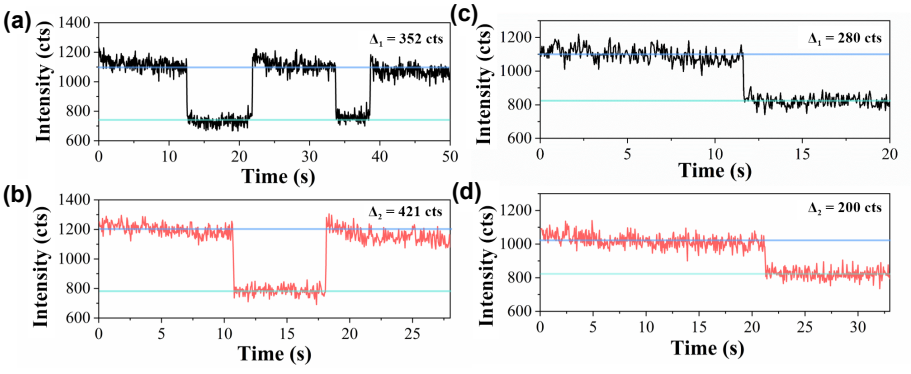

Figure 4 Chiral excitation dependence of middle-twisted NPLs. Emission time traces of a single middle-twisted NPL at room temperature under left-handed circularly polarized light (LCP) ((a), black) and right-handed circularly polarized light (RCP) ((b), red), with g factor of –0.178. Emission time traces of another single middle-twisted NPL under LCP ((c), black) and RCP ((d), red), with g factor of 0.333. The time traces are binned at 50 ms.

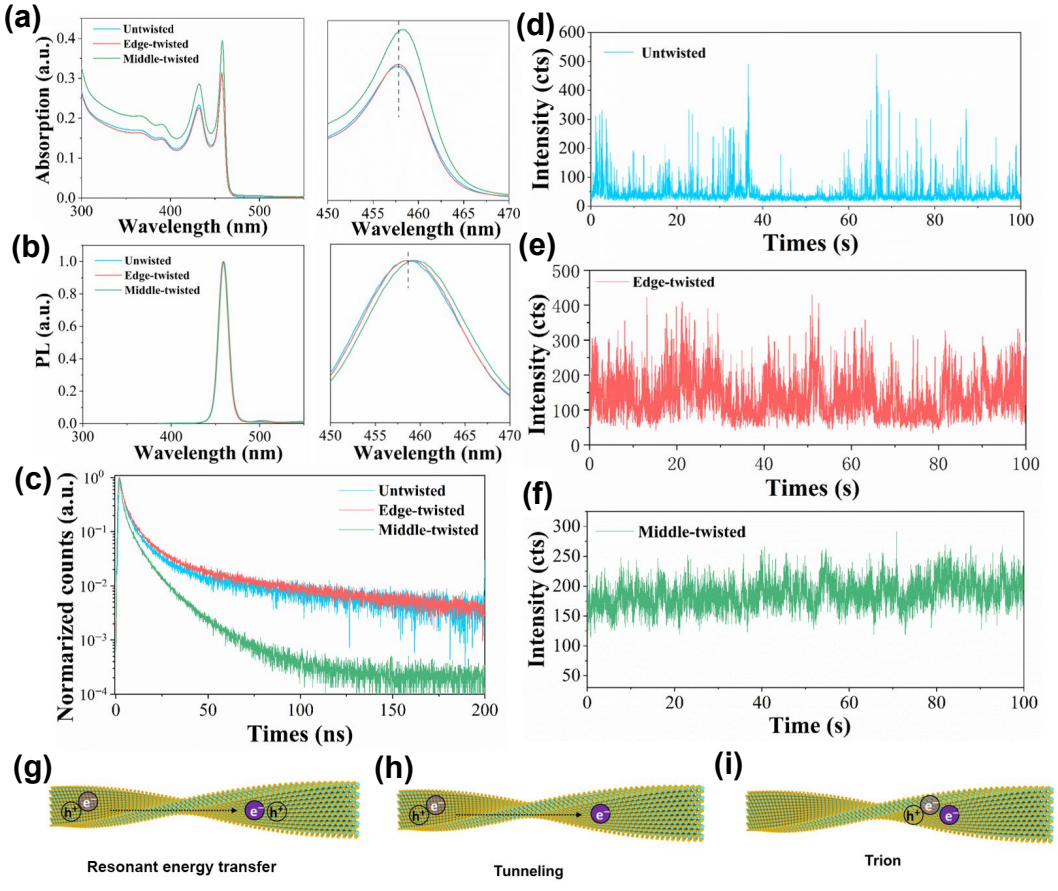

Figure 5 (a) and (b) Absorption and PL spectra of untwisted (blue), edge-twisted (red), and middle-twisted (green) NPLs. (c) PL lifetime decay curves of untwisted (blue), edge-twisted (red), and middle-twisted (green) NPLs. (d)–(f) Typical PL intensity trajectories of single untwisted (blue), edge-twisted (red), and middle-twisted (green) NPLs. The possible exciton dissociation pathway through resonant energy transfer (g) or via tunneling (h). (i) The excess carrier may occupy the region of the daughter NPL and form a trion.

with a much faster multiexponential decay compared with untwisted and edge-twisted NPLs (Fig. 5(c)).

These observations further suggest that quantum coupling takes place in middle-twisted NPLs and provide several important insights into understanding some fundamental questions: (1) Quenching of the radiative decay time related to coupling may be associated with tunneling between two daughter NPLs. For most quantum dots solids or double nanoparticles, the dipolar fluorescence resonance energy transfer (FRET) is dominant for the faster decay rate, which occurs before the successful recombination of the electron and hole (Fig. 5(g)) [46, 47]. For these organically linked nanoparticles, the tunneling effect of electrons through the high barrier of ligands is less prominent [47]. Twist splits one (parent) NPL into two daughter NPLs with no organic ligand stuck in the middle as the high potential barrier, where tunneling of the electron occurs (Fig. 5(h)). (2) The non-off emissive states in middle twisted NPLs arise due to efficient Auger suppression and accommodation of photogenerated trion states. Trions can either be negatively or positively charged because of their nature of three carriers (two electrons and one hole, or one electron and two holes) [48–51]. It has been reported that the emission spectra of NPLs show a significant contribution from trions at low temperatures [49, 52]. Alternatively, confinement potential engineering has been demonstrated as an efficient approach to suppress Auger recombination process and enhance trion emission [53]. Compared with nanocrystals, NPLs with their strong confinement in the thickness direction and extended lateral geometries exhibit large exciton coherence sizes and reduced carrier-carrier interactions that present an exciting opportunity for hosting trions [16]. In middle-twisted NPLs, the Auger rate is suppressed and the trions tend to become emissive. (3) In contrast to untwisted and edge-twisted NPLs, it is interesting to note that the middle-twisted structure exhibits more trions in their single-particle PL trajectories. The difference could be connected with a much softer confinement potential crested by twist compared to organic ligands in the middle [47]. In colloidal NPLs, carriers are strongly confined only along one dimension, where an electron-hole (e-h) pair is strongly bound and is expected to move together as an exciton at room temperature due to strong e-h Coulomb interaction [54]. In particular, after the creation of two daughter NPLs by twist, the excess carriers that confined only in one dimension of NPLs are free to rearrange in the lateral plane, and have more possibility to tunnel the twisted symmetric region to form a new type of trion (Fig. 5(i)), offering novel types of multicarrier configurations, and increasing the trion lifetime due to both structural and spatial separation as compared with untwisted and edge-twisted NPLs.

The current endeavor to develop coupled artificial molecules largely relies on the design of coupled nanocrystal structures, ranging from double quantum dots, dimers, to superlattices, in which quantum tunneling of charged carriers or dipole–dipole interactions of neutral carriers are exploited [41, 55]. For 2D colloidal NPLs, their potential as building blocks for molecular superstructures with quantum coupling remains unclear. The existence of inter NPLs excitations in coaxially stacked NPLs is evidenced by some primary constitutions [56, 57]. However, the quantum tunneling-driven coupling formation, analogous to epitaxial quantum well superlattices, is inhibited due to the large potential barrier (2–4 eV) imposed by the interlinking ligands [47]. We hereby, achieve this coupling by twist, which enables

twist one parent NPL into two daughter NPLs that are structurally and electronically coupled without any interlinking organic spacer layer. The electronic structures of these twisted NPLs can be modified by a robust route of twist and the dielectric environment can be altered by confined carriers polarized to the twisted symmetric one. These twisted NPLs are of great practical interest as an additional degree of freedom in the design of the electronic structures and possibly combine the excellent optical properties of NPLs with relevance toward diverse applications, especially quantum technologies.

4 Conclusions

In summary, we report the origin and propagation mechanism of twist in 2D CdSe NPLs during the colloidal growth process. The morphology of NPLs converts from totally flat to edge-twisted, and then to middle-twisted with the growth time of NPLs. The associated theoretical analysis shows the twist is length-dependent, with the critical length ~ 30 nm. We further explored the vital role of surface defects, which generate strong stress that causes a torsion and results in a twist. The circularly polarized characteristics of the middle-twisted NPLs were observed. The dissymmetry factor for middle-twisted NPLs up to 0.334 was achieved, which is much larger than that of the chiral NPLs synthesized by the ligand exchange method. Impressively, quantum coupling can be discerned in the middle-twisted NPLs by the redshift of the band gap transitions as well as single-particle circularly polarized excitation studies. Considering the variety of remarkable physical properties of twisted NPLs, such as chirality and quantum coupling, our work creates a framework for the further development of twistronics, quantum technologies, and optoelectronic applications.

Acknowledgements

This work was financially supported by the Beijing Natural Science Foundation (No. Z210018), the National Natural Science Foundation of China (Nos. 62105025, 12172047, 62127817, and 22173009), the Beijing Institute of Technology Research Fund Program for Young Scholars (No. 3040011182113). The authors would like to acknowledge the Experimental Center of Advanced Materials of Beijing Institute of Technology for the support in materials synthesis and characterization. We also acknowledge Dr. Xiangmin Hu for the helpful discussion. Theoretical calculations were performed using resources of the Supercomputer Centre in Chongqing.

Electronic Supplementary Material: Supplementary material (the analytical model for twist NPLs, first-principles calculations, and more TEM images of twisted NPLs) is available in the online version of this article at https://doi.org/10.1007/s12274-023-5529-x.

References

[1] Gao, P. X.; Ding, Y.; Mai, W. J.; Hughes, W. L.; Lao, C. S.; Wang, Z. L. Conversion of zinc oxide nanobelts into superlattice-structured nanohelices. *Science* **2005**, *309*, 1700–1704.

[2] Zhu, J.; Peng, H. L.; Marshall, A. F.; Barnett, D. M.; Nix, W. D.; Cui, Y. Formation of chiral branched nanowires by the Eshelby Twist. *Nat. Nanotechnol.* **2008**, *3*, 477–481.

[3] Srivastava, S.; Santos, A.; Critchley, K.; Kim, K. S.; Podsiadlo, P.; Sun, K.; Lee, J.; Xu, C. L.; Lilly, G. D.; Glotzer, S. C. et al. Light-controlled self-assembly of semiconductor nanoparticles into twisted ribbons. *Science* **2010**, *327*, 1355–1359.

[4] Cao, Y.; Rodan-Legrain, D.; Rubies-Bigorda, O.; Park, J. M.; Watanabe, K.; Taniguchi, T.; Jarillo-Herrero, P. Tunable correlated states and spin-polarized phases in twisted bilayer–bilayer graphene. *Nature* **2020**, *583*, 215–220.

[5] Turkel, S.; Swann, J.; Zhu, Z. Y.; Christos, M.; Watanabe, K.; Taniguchi, T.; Sachdev, S.; Scheurer, M. S.; Kaxiras, E.; Dean, C. R. et al. Orderly disorder in magic-angle twisted trilayer graphene. *Science* **2022**, *376*, 193–199.

[6] Dean, C. R.; Wang, L.; Maher, P.; Forsythe, C.; Ghahari, F.; Gao, Y.; Katoch, J.; Ishigami, M.; Moon, P.; Koshino, M. et al. Hofstadter's butterfly and the fractal quantum Hall effect in moiré superlattices. *Nature* **2013**, *497*, 598–602.

[7] Hunt, B.; Sanchez-Yamagishi, J. D.; Young, A. F.; Yankowitz, M.; LeRoy, B. J.; Watanabe, K.; Taniguchi, T.; Moon, P.; Koshino, M.; Jarillo-Herrero, P. et al. Massive Dirac fermions and Hofstadter butterfly in a van der Waals heterostructure. *Science* **2013**, *340*, 1427–1430.

[8] Cao, Y.; Fatemi, V.; Fang, S. A.; Watanabe, K.; Taniguchi, T.; Kaxiras, E.; Jarillo-Herrero, P. Unconventional superconductivity in magic-angle graphene superlattices. *Nature* **2018**, *556*, 43–50.

[9] Seyler, K. L. ; Rivera, P. ; Yu, H. Y. ; Wilson, N. P. ; Ray, E. L. ; Mandrus, D. G. ; Yan, J. Q. ; Yao, W. ; Xu, X. D. Signatures of moiré-trapped valley excitons in $MoSe_2/WSe_2$ heterobilayers. *Nature* **2019**, *567*, 66–70.

[10] Mishchenko, A.; Tu, J. S.; Cao, Y.; Gorbachev, R. V.; Wallbank, J. R.; Greenaway, M. T.; Morozov, V. E.; Morozov, S. V.; Zhu, M. J.; Wong, S. L. et al. Twist-controlled resonant tunnelling in graphene/boron nitride/graphene heterostructures. *Nat. Nanotechnol.* **2014**, *9*, 808–813.

[11] Hsu, W. T.; Zhao, Z. A.; Li, L. J.; Chen, C. H.; Chiu, M. H.; Chang, P. S.; Chou, Y. C.; Chang, W. H. Second harmonic generation from artificially stacked transition metal dichalcogenide twisted bilayers. *ACS Nano* **2014**, *8*, 2951–2958.

[12] Ribeiro-Palau, R.; Zhang, C. J.; Watanabe, K.; Taniguchi, T.; Hone, J.; Dean, C. R. Twistable electronics with dynamically rotatable heterostructures. *Science* **2018**, *361*, 690–693.

[13] Kang, K.; Lee, K. H.; Han, Y. M.; Gao, H.; Xie, S. E.; Muller, D. A.; Park, J. Layer-by-layer assembly of two-dimensional materials into wafer-scale heterostructures. *Nature* **2017**, *550*, 229–233.

[14] Pun, A. B.; Mazzotti, S.; Mule, A. S.; Norris, D. J. Understanding discrete growth in semiconductor nanocrystals: Nanoplatelets and magic-sized clusters. *Acc. Chem. Res.* **2021**, *54*, 1545–1554.

[15] Ithurria, S.; Dubertret, B. Quasi 2D colloidal CdSe platelets with thicknesses controlled at the atomic level. *J. Am. Chem. Soc.* **2008**, *130*, 16504–16505.

[16] Ithurria, S.; Tessier, M. D.; Mahler, B.; Lobo, R. P. S. M.; Dubertret, B.; Efros, A. L. Colloidal nanoplatelets with two-dimensional electronic structure. *Nat. Mater.* **2011**, *10*, 936–941.

[17] Ithurria, S.; Talapin, D. V. Colloidal atomic layer deposition (c-ALD) using self-limiting reactions at nanocrystal surface coupled to phase transfer between polar and nonpolar media. *J. Am. Chem. Soc.* **2012**, *134*, 18585–18590.

[18] Lhuillier, E.; Pedetti, S.; Ithurria, S.; Nadal, B.; Heuclin, H.; Dubertret, B. Two-dimensional colloidal metal chalcogenides semiconductors: Synthesis, spectroscopy, and applications. *Acc. Chem. Res.* **2015**, *48*, 22–30.

[19] Zhang, F. J.; Wang, S. J.; Wang, L.; Lin, Q. L.; Shen, H. B.; Cao, W. R.; Yang, C. C.; Wang, H. Z.; Yu, L.; Du, Z. L. et al. Super color purity green quantum dot light-emitting diodes fabricated by using CdSe/CdS nanoplatelets. *Nanoscale* **2016**, *8*, 12182–12188.

[20] Wen, Z. L.; Liu, P.; Ma, J. R.; Jia, S. Q.; Xiao, X. T.; Ding, S. H.; Tang, H. D.; Yang, H. C.; Zhang, C. J.; Qu, X. W. et al. High-performance ultrapure green CdSe/CdS core/crown nanoplatelet light-emitting diodes by suppressing nonradiative energy transfer. *Adv. Electron. Mater.* **2021**, *7*, 2000965.

[21] Li, Z.; Qin, H. Y.; Guzun, D.; Benamara, M.; Salamo, G.; Peng, X. G. Uniform thickness and colloidal-stable CdS quantum disks with tunable thickness: Synthesis and properties. *Nano Res.* **2012**, *5*, 337–351.

[22] She, C. X.; Fedin, I.; Dolzhnikov, D. S.; Demortière, A.; Schaller, R. D.; Pelton, M.; Talapin, D. V. Low-threshold stimulated emission using colloidal quantum wells. *Nano Lett.* **2014**, *14*, 2772–2777.

[23] Nasilowski, M.; Mahler, B.; Lhuillier, E.; Ithurria, S.; Dubertret, B.

Two-dimensional colloidal nanocrystals. *Chem. Rev.* **2016**, *116*, 10934–10982.

[24] Bouet, C.; Mahler, B.; Nadal, B.; Abecassis, B.; Tessier, M. D.; Ithurria, S.; Xu, X. Z.; Dubertret, B. Two-dimensional growth of CdSe nanocrystals, from nanoplatelets to nanosheets. *Chem. Mater.* **2013**, *25*, 639–645.

[25] Hutter, E. M.; Bladt, E.; Goris, B.; Pietra, F.; van der Bok, J. C.; Boneschanscher, M. P.; de Mello Donegá, C.; Bals, S.; Vanmaekelbergh, D. Conformal and atomic characterization of ultrathin CdSe platelets with a helical shape. *Nano Lett.* **2014**, *14*, 6257–6262.

[26] Jana, S.; de Frutos, M.; Davidson, P.; Abécassis, B. Ligand-induced twisting of nanoplatelets and their self-assembly into chiral ribbons. *Sci. Adv.* **2017**, *3*, e1701483.

[27] Vasiliev, R. B.; Lazareva, E. P.; Karlova, D. A.; Garshev, A. V.; Yao, Y. Z.; Kuroda, T.; Gaskov, A. M.; Sakoda, K. Spontaneous folding of CdTe nanosheets induced by ligand exchange. *Chem. Mater.* **2018**, *30*, 1710–1717.

[28] Kim, W. D.; Yoon, D. E.; Kim, D.; Koh, S.; Bae, W. K.; Chae, W. S.; Lee, D. C. Stacking of colloidal CdSe nanoplatelets into twisted ribbon superstructures: Origin of twisting and its implication in optical properties. *J. Phys. Chem. C* **2019**, *123*, 9445–9453.

[29] Liu, Y. Y.; Rowell, N.; Willis, M.; Zhang, M.; Wang, S. L.; Fan, H. S.; Huang, W.; Chen, X. Q.; Yu, K. Photoluminescent colloidal nanohelices self-assembled from CdSe magic-size clusters via nanoplatelets. *J. Phys. Chem. Lett.* **2019**, *10*, 2794–2801.

[30] Guillemeney, L.; Lermusiaux, L.; Landaburu, G.; Wagnon, B.; Abécassis, B. Curvature and self-assembly of semi-conducting nanoplatelets. *Commun. Chem.* **2022**, *5*, 7.

[31] Castro, N.; Bouet, C.; Ithurria, S.; Lequeux, N.; Constantin, D.; Levitz, P.; Pontoni, D.; Abécassis, B. Insights into the formation mechanism of CdSe nanoplatelets using *in situ* X-ray scattering. *Nano Lett.* **2019**, *19*, 6466–6474.

[32] Po, H.; Dabard, C.; Roman, B.; Reyssat, E.; Bico, J.; Baptiste, B.; Lhuillier, E.; Ithurria, S. Chiral helices formation by self-assembled molecules on semiconductor flexible substrates. *ACS Nano* **2022**, *16*, 2901–2909.

[33] Di Giacomo, A.; Rodà, C.; Khan, A. H.; Moreels, I. Colloidal synthesis of laterally confined blue-emitting 3. 5 monolayer CdSe nanoplatelets. *Chem. Mater.* **2020**, *32*, 9260–9267.

[34] Singh, S.; Tomar, R.; Ten Brinck, S.; De Roo, J.; Geiregat, P.; Martins, J. C.; Infante, I.; Hens, Z. Colloidal CdSe nanoplatelets, a model for surface chemistry/optoelectronic property relations in semiconductor nanocrystals. *J. Am. Chem. Soc.* **2018**, *140*, 13292–13300.

[35] Yeom, J.; Yeom, B.; Chan, H.; Smith, K. W.; Dominguez-Medina, S.; Bahng, J. H.; Zhao, G. P.; Chang, W. S.; Chang, S. J.; Chuvilin, A. et al. Chiral templating of self-assembling nanostructures by circularly polarized light. *Nat. Mater.* **2015**, *14*, 66–72.

[36] Wang, P. P.; Yu, S. J.; Govorov, A. O.; Ouyang, M. Cooperative expression of atomic chirality in inorganic nanostructures. *Nat. Commun.* **2017**, *8*, 14312.

[37] Vinegrad, E.; Vestler, D.; Ben-Moshe, A.; Barnea, A. R.; Markovich, G.; Cheshnovsky, O. Circular dichroism of single particles. *ACS Photonics* **2018**, *5*, 2151–2159.

[38] Sang, Y. T.; Han, J. L.; Zhao, T. H.; Duan, P. F.; Liu, M. H. Circularly polarized luminescence in nanoassemblies: Generation, amplification, and application. *Adv. Mater.* **2020**, *32*, 1900110.

[39] Lee, H. E.; Ahn, H. Y.; Mun, J.; Lee, Y. Y.; Kim, M.; Cho, N. H.; Chang, K.; Kim, W. S.; Rho, J.; Nam, K. T. Amino-acid- and peptide-directed synthesis of chiral plasmonic gold nanoparticles. *Nature* **2018**, *556*, 360–365.

[40] Yang, G. L.; Kazes, M.; Oron, D. Chiral 2D colloidal semiconductor quantum wells. *Adv. Funct. Mater.* **2018**, *28*, 1802012.

[41] Cui, J. B.; Panfil, Y. E.; Koley, S.; Shamalia, D.; Waiskopf, N.; Remennik, S.; Popov, I.; Oded, M.; Banin, U. Colloidal quantum dot molecules manifesting quantum coupling at room temperature. *Nat. Commun.* **2019**, *10*, 5401.

[42] Kuo, Y. H.; Lee, Y. K.; Ge, Y. S.; Ren, S.; Roth, J. E.; Kamins, T. I.; Miller, D. A. B.; Harris, J. S. Strong quantum-confined Stark effect in germanium quantum-well structures on silicon. *Nature* **2005**, *437*, 1334–1336.

[43] Tessier, M. D.; Javaux, C.; Maksimovic, I.; Loriette, V.; Dubertret, B. Spectroscopy of single CdSe nanoplatelets. *ACS Nano* **2012**, *6*, 6751–6758.

[44] Tessier, M. D.; Mahler, B.; Nadal, B.; Heuclin, H.; Pedetti, S.; Dubertret, B. Spectroscopy of colloidal semiconductor core/shell nanoplatelets with high quantum yield. *Nano Lett.* **2013**, *13*, 3321–3328.

[45] Amgar, D.; Yang, G. L.; Tenne, R.; Oron, D. Higher-order photon correlation as a tool to study exciton dynamics in quasi-2D nanoplatelets. *Nano Lett.* **2019**, *19*, 8741–8748.

[46] Teitelboim, A.; Meir, N.; Kazes, M.; Oron, D. Colloidal double quantum dots. *Acc. Chem. Res.* **2016**, *49*, 902–910.

[47] Choi, J. J.; Luria, J.; Hyun, B. R.; Bartnik, A. C.; Sun, L. F.; Lim, Y. F.; Marohn, J. A.; Wise, F. W.; Hanrath, T. Photogenerated exciton dissociation in highly coupled lead salt nanocrystal assemblies. *Nano Lett.* **2010**, *10*, 1805–1811.

[48] Park, Y. S.; Bae, W. K.; Pietryga, J. M.; Klimov, V. I. Auger recombination of biexcitons and negative and positive trions in individual quantum dots. *ACS Nano* **2014**, *8*, 7288–7296.

[49] Shornikova, E. V.; Yakovlev, D. R.; Biadala, L.; Crooker, S. A.; Belykh, V. V.; Kochiev, M. V.; Kuntzmann, A.; Nasilowski, M.; Dubertret, B.; Bayer, M. Negatively charged excitons in CdSe nanoplatelets. *Nano Lett.* **2020**, *20*, 1370–1377.

[50] Ayari, S.; Quick, M. T.; Owschimikow, N.; Christodoulou, S.; Bertrand, G. H. V.; Artemyev, M.; Moreels, I.; Woggon, U.; Jaziri, S.; Achtstein, A. W. Tuning Trion binding energy and oscillator strength in a laterally finite 2D system: CdSe nanoplatelets as a model system for Trion properties. *Nanoscale* **2020**, *12*, 14448–14458.

[51] Li, J. L.; Wang, D. F.; Zhang, G. F.; Yang, C. G.; Guo, W. L.; Han, X.; Bai, X. Q.; Chen, R. Y.; Qin, C. B.; Hu, J. Y. et al. The role of surface charges in the blinking mechanisms and quantum-confined Stark effect of single colloidal quantum dots. *Nano Res.* **2022**, *15*, 7655–7661.

[52] Peng, L. T.; Otten, M.; Hazarika, A.; Coropceanu, I.; Cygorek, M.; Wiederrecht, G. P.; Hawrylak, P.; Talapin, D. V.; Ma, X. D. Bright Trion emission from semiconductor nanoplatelets. *Phys. Rev. Mater.* **2020**, *4*, 056006.

[53] Cragg, G. E.; Efros, A. L. Suppression of auger processes in confined structures. *Nano Lett.* **2010**, *10*, 313–317.

[54] Kunneman, L. T.; Tessier, M. D.; Heuclin, H.; Dubertret, B.; Aulin, Y. V.; Grozema, F. C.; Schins, J. M.; Siebbeles, L. D. A. Bimolecular auger recombination of electron-hole pairs in two-dimensional CdSe and CdSe/CdZnS core/shell nanoplatelets. *J. Phys. Chem. Lett.* **2013**, *4*, 3574–3578.

[55] Jia, G. H.; Sitt, A.; Hitin, G. B.; Hadar, I.; Bekenstein, Y.; Amit, Y.; Popov, I.; Banin, U. Couples of colloidal semiconductor nanorods formed by self-limited assembly. *Nat. Mater.* **2014**, *13*, 301–307.

[56] Guzelturk, B.; Erdem, O.; Olutas, M.; Kelestemur, Y.; Demir, H. V. Stacking in colloidal nanoplatelets: Tuning excitonic properties. *ACS Nano* **2014**, *8*, 12524–12533.

[57] Diroll, B. T.; Cho, W.; Coropceanu, I.; Harvey, S. M.; Brumberg, A.; Holtgrewe, N.; Crooker, S. A.; Wasielewski, M. R.; Prakapenka, V. B.; Talapin, D. V. et al. Semiconductor nanoplatelet excimers. *Nano Lett.* **2018**, *18*, 6948–6953.